Low-frequency spin dynamics in the orthorombic phase of La_2CuO_4

J. Chovan[1,2] and N. Papanicolaou[1,a]

[1]*Department of Physics, University of Crete, and Research Center of Crete, Heraklion, Greece*
[2]*Faculty of Science, P.J.Šafárik University, Park Angelinum 9, 04154 Košice, Slovakia*

Abstract. An effective field theory is derived that describes the low-frequency spin dynamics in the low-temperature orthorombic phase of La_2CuO_4. Restricted to a single CuO_2 layer the effective theory is a simple generalization of the relativistic nonlinear σ model to include all spin interactions allowed by symmetry. Incorporating a weak interlayer interaction leads to two coupled nonlinear σ models which provide an efficient description of the complete bilayer dynamics. Particular attention is paid to the weak-ferromagnetic and spin-flop transitions induced by external magnetic fields. The main features of the observed (covert) weak ferromagnetism are thus accounted for in a straight-forward manner but some of the finer theoretical predictions would require further experimental investigation. The derived framework is also suitable for the study of the structure and dynamics of magnetic domains in undoped La_2CuO_4.

I. INTRODUCTION

The magnetic properties of La_2CuO_4 have been extensively studied during the last decade [1]. In a crude approximation this system is described by a two-dimensional (2D) isotropic Heisenberg antiferromagnet. However the orthorombic distortion of the crystal that takes place below $530K$ induces anisotropic spin couplings, the most important of which is a Dzyaloshinskii-Moriya (DM) anisotropy [2,3] that should lead to spin canting and thus weak ferromagnetism. Yet a small antiferromagnetic interlayer coupling forces successive CuO_2 layers to cant in opposite direction and the induced weak moments average to zero in the absence of external fields. Nevertheless the sustained experimental as well as theoretical effort of Thio et al. [4–6] established that La_2CuO_4 is indeed a covert weak ferromagnet.

The derived phenomenological picture was further probed by symmetry analysis [7,8] and by a fresh and challenging look at the DM anisotropy due to Kaplan [9] and Shekhtman, Entin-Wohlman, and Aharony [10,11]. The main outcome of the latter work is sometimes referred to as the KSEA anisotropy and is the subject of current experimental investigation in the related context of helimagnetism [12].

Our purpose is to systematize the above developments into a simple field theoretical framework that should facilitate further work on this interesting subject. The relevance of effective field theories became apparent through standard hydrodynamic approaches [13,14] which eventually led to a successful description of the isotropic Heisenberg antiferromagnet in terms of a relativistic nonlinear σ model [15,16]. A similar approach has been employed for the study of the dynamics of domain walls and related topological magnetic solitons in conventional weak ferromagnets [17]. This issue has remained largely unexplored in the cuprates, apparently due to the hidden nature of weak ferromagnetism and a corresponding lack of a complete field theoretical description.

In Section 2 we repeat the symmetry analysis to obtain the most general spin Hamiltonian involving nearest-neighbor (nn) interactions. Based on this Hamiltonian we proceed with the derivation of an effective field theory valid at low frequencies in two steps. First, in Section 3, we derive a suitable extension of the 2D nonlinear σ model which would be appropriate for the description of a single CuO_2 layer provided that the interlayer coupling could be neglected. Second, in Section 4, we incorporate a weak interlayer interaction to obtain the final effective theory in the form of two coupled nonlinear σ models. The main phenomenological implications are also worked out in Section 4, including a discussion of the observed weak-ferromagnetic [4] and spin-flop [5] transitions. Our conclusions are summarized in Section 5 by listing those issues that seem to deserve further attention. In the Appendix we derive the most general next-nearest-neighbor (nnn) in-plane interaction compatible with symmetry.

II. SYMMETRY CONSTRAINTS

The crystal structure of La_2CuO_4 has been discussed on several occasions and the accumulated information is freely used in this section. In particular, we found the expositions of references [18,19] lucid and informative. The crystal undergoes a structural phase transition from a tetragonal ($I4/mmm$) phase at high temperatures to an orthorombic ($Bmab$) phase below $530K$. Throughout this paper we confine attention to the low-temperature orthorombic (LTO) phase.

The relevant space group $Bmab$ is usually listed as $Cmca$ in standard tables of crystallography using a slightly different choice of conventions. Our conventions are illustrated in Figure 1 which depicts the orthorombic

unit cell stripped of all but the magnetic sites; i.e., the positions of the spin $s = 1/2$ Cu^{2+} ions. Dashed lines in this figure join nn neighbors within each CuO_2 plane and are the descendants of the original tetragonal axes which are no longer orthogonal due to the orthorhombic distortion. In a first approximation, the magnetic ground state is such that spins at sites denoted by A and Δ point along the positive (negative) b axis, while spins at B and Γ point along the negative (positive) b axis [20]. However, when anisotropies and a weak interlayer coupling are taken into account, each spin suffers a slight canting which leads to four inequivalent magnetic sites and a corresponding four-sublattice picture. In the following, spin vectors are denoted by their standard symbol $\mathbf{S}$, or by $\mathbf{A}, \mathbf{B}, \mathbf{\Gamma}, \mathbf{\Delta}$ when a distinction among the four sublattices becomes necessary.
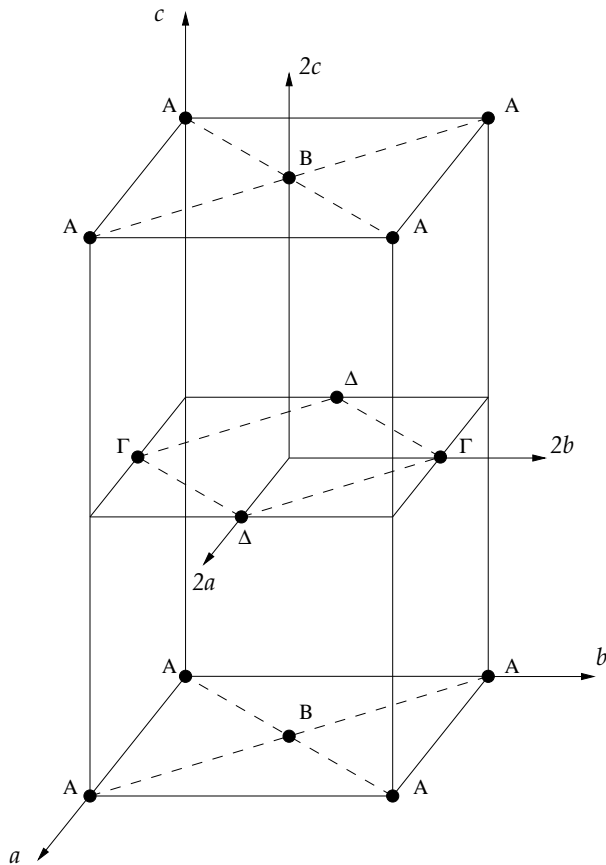

FIG. 1. The orthorombic unit cell of La_2CuO_4 stripped of all but the Cu atoms denoted by solid circles. Dashed lines join nn neighbors within each CuO_2 plane and are the descendants of the original tetragonal axes. The four inequivalent magnetic sites are labeled by A, B, Γ and Δ.

In order to list the symmetry elements of the space group we begin with the most general primitive translation

$$\mathbf{T} = \alpha a \mathbf{e}_a + \beta b \mathbf{e}_b + \gamma c \mathbf{e}_c, \qquad (1)$$

where $\mathbf{e}_a$, $\mathbf{e}_b$ and $\mathbf{e}_c$ are unit vectors along the crystal axes, $a = 5.35 \mathring{A}$, $b = 5.40 \mathring{A}$ and $c = 13.15 \mathring{A}$ are the lattice constants, and (α, β, γ) is a set of integers that may also be used to label the relative position of a unit cell through the Cartesian coordinates $x = \alpha a, y = \beta b$ and $z = \gamma c$. We further consider the two fractional translations

$$\tau = \frac{1}{2}(a\mathbf{e}_a + c\mathbf{e}_c), \qquad \tau' = \frac{1}{2}(a\mathbf{e}_a + b\mathbf{e}_b), \qquad (2)$$

where τ is in itself a symmetry operation. The symmetry group of the unit cell is then written symbolically as $G = G_0 + \tau \times G_0$ where G_0 contains the eight elements

$$E, I, \sigma_a, \sigma_b', \sigma_c', C_{2a}, C_{2b}', C_{2c}'. \qquad (3)$$

Here E denotes identity, I inversion about a Cu site, $\sigma_a, \sigma_b, \sigma_c$ reflections about the planes $x = a/2$, $y = b/2$, $z = c/2$, and C_{2a}, C_{2b}, C_{2c} 180° rotations around the axes that emanate from the center of the unit cell as shown in Figure 1. Primed elements in equation (3) must be complemented by the special fractional translation τ' which is *not* in itself a symmetry operation. Finally we note that all elements of G can be generated from the fundamental set $(\tau, I, \sigma_a, C_{2c}')$ by suitable group multiplications. The above four elements have been used to derive the spin Hamiltonian described in the remainder of this section without presenting the detailed symmetry arguments.

We first discuss a 2D restriction that would be appropriate for the description of a single CuO_2 layer if the interlayer coupling could be neglected. The special symmetry element τ of equation (2) maps AB bonds in the basal plane to $\Gamma\Delta$ bonds in the middle plane. Therefore it is sufficient to consider for the moment only the basal plane. We assume that the Hamiltonian contains terms that are at most quadratic in the spin operators, even though quartic terms are occasionally invoked to explain some features of multimagnon dynamics [21]. Including all nn interactions within the plane the Hamiltonian is written as the sum of four terms :

$$W = W_E + W_{DM} + W_A + W_Z, \qquad (4)$$

which we now describe in detail. The first term

$$W_E = \sum_{<kl>} J_{kl}(\mathbf{S}_k \cdot \mathbf{S}_l) \qquad (5)$$

contains the isotropic exchange interaction over nn in-plane bonds denoted by $< kl >$. Symmetry requires that

$$J_{kl} = J, \qquad \text{for all in−plane nn bonds.} \qquad (6)$$

The second term

$$W_{DM} = \sum_{<kl>} \mathbf{D}_{kl} \cdot (\mathbf{S}_k \times \mathbf{S}_l) \qquad (7)$$

is the standard (antisymmetric) DM anisotropy [2,3]. The vectors $\mathbf{D}_{kl}$ are severely restricted by symmetry and take only two distinct values:

$$\mathbf{D}_1 = D\mathbf{e}_a + D'\mathbf{e}_b, \qquad \mathbf{D}_2 = D\mathbf{e}_a - D'\mathbf{e}_b, \qquad (8)$$

which are distributed over the 2D lattice as shown in Figure 2 where a sign alternation $\pm\mathbf{D}_1$ and $\pm\mathbf{D}_2$ on opposite bonds is also displayed. This alternation together with the specific form of DM vectors (8) were derived by Coffey, Bedell, and Trugman [7]. Actually the DM vectors given in the above reference differ from those of equation (8) by a 45° rotation, apparently because they were referred to the original tetragonal axes. Since the latter axes are not exactly orthogonal in the LTO phase, statement (8) should be viewed as slightly more precise. The third term

$$W_A = \frac{1}{2} \sum_{<kl>} \sum_{i,j} K_{kl}^{ij}(S_k^i S_l^j + S_k^j S_l^i) \qquad (9)$$

encompasses all "symmetric" exchange anisotropies over nn in-plane bonds. Again the matrices K_{kl} are restricted by symmetry to two possible values:

$$K_1 = \begin{pmatrix} K_{aa} & K_{ab} & 0 \\ K_{ab} & K_{bb} & 0 \\ 0 & 0 & K_{cc} \end{pmatrix},$$

$$K_2 = \begin{pmatrix} K_{aa} & -K_{ab} & 0 \\ -K_{ab} & K_{bb} & 0 \\ 0 & 0 & K_{cc} \end{pmatrix}, \qquad (10)$$

which are distributed as shown in Figure 2. The above matrices may be taken to be traceless ($K_{aa}+K_{bb}+K_{cc} = 0$) because the isotropic component of the exchange interaction has already been accounted for by equation (5). Finally the fourth term

$$W_Z = -\sum_l (\mathbf{H} \cdot \mathbf{S}_l) \qquad (11)$$

is simply the Zeeman interaction produced by an external field $\mathbf{H}$.

The symmetry analysis was further extended to include all nnn in-plane interactions; namely, couplings along the diagonals of the Cu plaquettes which are parallel to the orthorhombic a and b axes. The resulting additions to the Hamiltonian are summarized in the Appendix. However, although we have kept track of the nnn interactions throughout our analysis, the corresponding results will not be included in the main text because we wish to keep the exposition reasonably simple. But we will occasionally mention potential contributions from the nnn interactions.

We next turn our attention to possible microscopic mechanisms that produce the various anisotropies. A good starting point is the KSEA Hamiltonian [11]
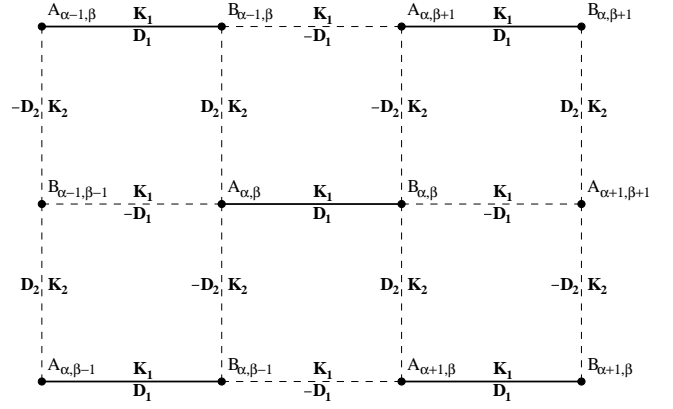

FIG. 2. Illustration of the distribution of the DM vectors $\pm\mathbf{D}_1$ and $\pm\mathbf{D}_2$, and of the symmetric exchange matrices K_1 and K_2, on a portion of the basal plane. The spins $\mathbf{A}$ and $\mathbf{B}$ in a given dimer are labeled by a pair of indices (α, β) that advance along the orthorhombic axes a and b not shown in the figure.

$$W = \sum_{<kl>} \Big[\, (J_{kl} - \frac{|\mathbf{D}_{kl}|^2}{4J_{kl}})(\mathbf{S}_k \cdot \mathbf{S}_l) + \mathbf{D}_{kl} \cdot (\mathbf{S}_k \times \mathbf{S}_l)$$
$$+ \frac{1}{2J_{kl}}(\mathbf{S}_k \cdot \mathbf{D}_{kl})(\mathbf{D}_{kl} \cdot \mathbf{S}_l) \,\Big], \qquad (12)$$

obtained by carrying the perturbative treatment of spin-orbit interaction to second order. The second-order terms in equation (12) are usually neglected by comparison to the linear DM anisotropy. However their effect can be far more subtle noting that the total contribution from each specific mode can be brought to a completely isotropic form by rotating the spin operators $\mathbf{S}_k$ and $\mathbf{S}_l$ around the $\mathbf{D}_{kl}$ axis with angles $-\theta_{kl}$ and θ_{kl} such that $\tan\theta_{kl} = |\mathbf{D}_{kl}|^2/2J_{kl}$. One would naively conclude that Hamiltonian (12) does not predict spin ordering of any kind; in particular, weak ferromagnetism. Nevertheless spin ordering may occur as a result of frustration when the collective effect from all bonds is taken into account. This delicate line of reasoning [11] led to some interesting predictions such as the existence of weak ferromagnetism in the LTO phase of pure La_2CuO_4 but its absence in the low-temperature tetragonal (LTT, space group $P4_2/ncm$) phase that may be realized in, say, Ba-doped $La_{2-x}Ba_xCuO_4$.

It should be expected that the exchange anisotropy abstracted from equation (12) is consistent with the symmetry statement (10). Indeed, taking into account that $J_{kl} = J$ for all in-plane bonds and the specific form of the DM vectors from equation (8), the (traceless) KSEA anisotropy is found to be a special case of (10) with

$$K_{aa} = \frac{2D^2 - D'^2}{6J}, \qquad K_{bb} = \frac{2D'^2 - D^2}{6J},$$

$$K_{cc} = -\frac{D^2 + D'^2}{6J}, \qquad K_{ab} = \frac{DD'}{2J}, \qquad (13)$$

3

Of course, spin-orbit interaction is not the only source of anisotropy and, in fact, Coulomb exchange produces an Ising-like term [11,22] described by

$$K_{aa} = \frac{1}{3}K = K_{bb}, \qquad K_{cc} = -\frac{2}{3}K, \qquad (14)$$

which should be added to the corresponding elements of equation (13). Therefore we proceed with caution using the most general anisotropy given by equation (10) and return to further discussion of the special cases (13) and (14) after the dust settles, in Section 3.

The remainder of this section is devoted to a brief explanation of our main strategy. At this point we invoke the classical approximation, the validity of which will not be questioned until Section 4. The 2D dynamics will thus be described by the Landau-Lifshitz equation [23] in the form given by Gilbert [24]:

$$\frac{\partial \mathbf{A}}{\partial t} + \gamma(\mathbf{A} \times \frac{\partial \mathbf{A}}{\partial t}) = \mathbf{A} \times \mathbf{F}_A, \quad \mathbf{F}_A = -\frac{\partial W}{\partial \mathbf{A}},$$

$$\frac{\partial \mathbf{B}}{\partial t} + \gamma(\mathbf{B} \times \frac{\partial \mathbf{B}}{\partial t}) = \mathbf{B} \times \mathbf{F}_B, \quad \mathbf{F}_B = -\frac{\partial W}{\partial \mathbf{B}}, \quad (15)$$

where γ is a dissipation constant. The spin variables $\mathbf{A}$ and $\mathbf{B}$ are treated as classical vectors of length s, and the lattice indices (α, β) displayed in Figure 2 are suppressed in equation (15) for notational convenience.

The suppression of indices is more than symbolic if one wishes to study only the homogeneous spin dynamics in the presence of a spatially uniform field $\mathbf{H}$. Then spins assume only two distinct values $\mathbf{A}$ and $\mathbf{B}$, one for each sublattice, and the effective fields $\mathbf{F}_A$ and $\mathbf{F}_B$ in equation (15) may be derived from the much simpler Hamiltonian

$$\begin{aligned} W_C = 4[&J(\mathbf{A} \cdot \mathbf{B}) + D(A_b B_c - A_c B_b) \\ &+ K_{aa}A_a B_a + K_{bb}A_b B_b + K_{cc}A_c B_c] \\ &- \mathbf{H} \cdot (\mathbf{A} + \mathbf{B}), \end{aligned} \qquad (16)$$

where (A_a, A_b, A_c) and (B_a, B_b, B_c) are the Cartesian components of the spin vectors $\mathbf{A}$ and $\mathbf{B}$ along the orthorhombic axes. A notable fact is that neither D' nor K_{ab} enter equation (16). If we further restrict the diagonal anisotropies to the Ising form (14), equation (16) yields the unit-cell Hamiltonian employed by Thio et al. to account for a wide range of experiments [4–6]. The sign alternation of the DM vectors on opposite bonds [7] is crucial for the description in terms of a unit-cell Hamiltonian and was thus implicitly assumed in reference [4]. Lack of sign alternation would lead to spiral magnetic order or helimagnetism [12].

The information accumulated so far is employed in Section 3 to study the 2D dynamics of a single layer. One should recall that the dynamics of the middle plane is completely isomorphic and may be obtained by the simple substitution $(\mathbf{A}, \mathbf{B}) \rightarrow (\mathbf{\Gamma}, \mathbf{\Delta})$. The complete 3D dynamics including interlayer interactions will be studied in Section 4.

III. DYNAMICS OF A SINGLE LAYER

The unit-cell Hamiltonian (16) may be analyzed through the classical Landau-Lifshitz equations (15) to furnish explicit predictions for the characteristic magnon frequencies and the corresponding dynamic susceptibilities, following the early treatment of orthoferrites by Herrmann [25,26]. Considerable simplifications are invoked along the way by appealing to the phenomenological fact that anisotropies and the applied field are much smaller than the isotropic exchange constant:

$$D, K, H \ll J. \qquad (17)$$

Simply stated our task is to derive an effective low-frequency dynamics in which the strong inequalities (17) are taken into account from the outset. And, at little extra cost, we aim to go beyond the homogeneous dynamics to include spatial variations within a complete continuum field theory in the form of a nonlinear σ model.

One must thus deal with the complete discrete Landau-Lifshitz equations (15) where $\mathbf{A} = \mathbf{A}_{\alpha,\beta}$ and $\mathbf{B} = \mathbf{B}_{\alpha,\beta}$ are the spin vectors in a generic dimer labeled by two integers (α, β) that advance along the orthorhombic a and b axes, as shown in Figure 2. The corresponding effective fields $\mathbf{F}_A$ and $\mathbf{F}_B$ are then constructed by closely following the prescription for the complete microscopic Hamiltonian (4) given in Section 2. The resulting algebraic expressions are somewhat lengthy but the actual derivation is a straightforward adaptation of a direct method employed earlier for the study of an 1D model weak ferromagnet [27] and a 2D antiferromagnet [28]. We thus suppress the algebraic details and state the final result which can be explained in a simple manner.

Rationalized space-time variables are defined from

$$\eta = \alpha\delta, \qquad \xi = \beta\delta, \qquad \tau = 2s\delta Jt, \qquad (18)$$

where δ is a dimensionless scale whose significance will be made precise as the argument progresses. The actual distances along the a and b axes are then given by $x = \eta a/\delta$ and $y = \xi b/\delta$ while frequency is measured in units of $2s\delta J$. We also define rescaled parameters grouped into two categories. The DM anisotropy and the applied field are scaled linearly with δ :

$$d = \frac{2D}{\delta J}, \qquad \mathbf{h} = \frac{\mathbf{H}}{2s\delta J}, \qquad (19)$$

whereas diagonal anisotropies are scaled quadratically:

$$\kappa_a = \frac{8K_{aa}}{\delta^2 J}, \qquad \kappa_b = \frac{8K_{bb}}{\delta^2 J}, \qquad \kappa_c = \frac{8K_{cc}}{\delta^2 J}. \qquad (20)$$

Note that the parameters D' and K_{ab} do not appear in the above list because they eventually drop out of the effective low-frequency dynamics, for essentially the same reason they do not appear in the unit-cell Hamiltonian (16).

4

Concerning the field variables a transparent formulation is obtained in terms of the "magnetization" $\mathbf{m}$ and the "staggered magnetization" $\mathbf{n}$ which are defined by

$$\mathbf{m} = \frac{1}{2s}(\mathbf{A} + \mathbf{B}), \qquad \mathbf{n} = \frac{1}{2s}(\mathbf{A} - \mathbf{B}), \qquad (21)$$

and satisfy the classical constraints $\mathbf{m} \cdot \mathbf{n} = 0$ and $\mathbf{m}^2 + \mathbf{n}^2 = 1$. The basis for the derivation of an effective field theory is that the strong inequalities (17) imply $|\mathbf{m}| \ll |\mathbf{n}|$. Indeed, a consistent low-frequency reduction of the Landau-Lifshitz equation is obtained by treating $\mathbf{m}$ as a quantity of order δ, whereas the staggered moment $\mathbf{n}$ and the rescaled variables (19)-(21) are assumed to be of order unity. Then, to leading order, the classical constraints reduce to

$$\mathbf{m} \cdot \mathbf{n} = 0, \qquad \mathbf{n}^2 = 1, \qquad (22)$$

and $\mathbf{m}$ may be expressed in terms of $\mathbf{n}$ through the algebraic relation

$$\mathbf{m} = \frac{\delta}{4}[\mathbf{n} \times (\dot{\mathbf{n}} + \mathbf{d} - \mathbf{n} \times \mathbf{h}) - (\mathbf{n}_\eta + \mathbf{n}_\xi)], \qquad (23)$$

where $\mathbf{d} = d\mathbf{e}_a$, the dot denotes differentiation with respect to τ, and subscripts differentiation with respect to the spatial coordinates η and ξ. The various pieces of equation (23) have appeared in earlier studies of conventional weak ferromagnets [17,27] and antiferromagnets [28] and will not be discussed here in detail.

The main point is that the dynamical equations may now be stated entirely in terms of the staggered moment $\mathbf{n}$ which satisfies the nonlinear σ model

$$\mathbf{n} \times (\mathbf{f} + \lambda \dot{\mathbf{n}}) = 0, \qquad \mathbf{n}^2 = 1, \qquad (24)$$

where $\lambda = 4s\gamma/\delta$ is a rescaled dissipation constant, and the effective field $\mathbf{f}$ may be derived from an action principle :

$$\mathbf{f} = -\frac{\delta \mathcal{A}}{\delta \mathbf{n}}, \qquad \mathcal{A} = \int L \, d\eta d\xi d\tau, \qquad (25)$$

where $\mathcal{A}$ is the action and L the corresponding Lagrangian density

$$L = L_0 - V. \qquad (26)$$

Here L_0 is the "free" Lagrangian

$$L_0 = \frac{1}{2}(\dot{\mathbf{n}}^2 - \mathbf{n}_\eta^2 - \mathbf{n}_\xi^2) + \mathbf{h} \cdot (\mathbf{n} \times \dot{\mathbf{n}}) \qquad (27)$$

and V is the "potential"

$$V = (\mathbf{h} \times \mathbf{d}) \cdot \mathbf{n} + \frac{1}{2}(\mathbf{n} \cdot \mathbf{h})^2 + \frac{1}{2}(a_1^2 n_a^2 + a_2^2 n_c^2), \qquad (28)$$

where (n_a, n_b, n_c) are the Cartesian components of $\mathbf{n}$ and

$$a_1^2 = d^2 + \kappa_b - \kappa_a, \qquad a_2^2 = \kappa_b - \kappa_c, \qquad (29)$$

are the final effective anisotropy constants.

If the applied field were absent ($\mathbf{h} = 0$) the derived field theory would be relativistically invariant. The "velocity of light" is equal to the magnon velocity in the corresponding isotropic antiferromagnet and is scaled out of equation (27) thanks to the use of rationalized units. Recalling that $x = \eta a/\delta$, $y = \xi b/\delta$, and $\tau = 2s\delta J$, the actual magnon velocities along the a and b directions are $V_a = 2saJ$ and $V_b = 2sbJ$. The predicted slight anisotropy $V_b/V_a = 1.01$ cannot be discerned in current experiments which yield an average spinwave velocity $V_{sw} \approx V_a \approx V_b \approx 850 meV\mathring{A}$ for pure La_2CuO_4 samples [1]. Using an average lattice constant $a \approx b = 5.375\mathring{A}$ one may extract a classical value for the exchange constant $J = 158 meV$ which differs from the usually accepted $J = 135 meV$ by the calculated quantum-renormalization factor 1.18.

We are now in a position to make contact with the various special limits of the exchange anisotropy discussed in Section 2. The pure Ising anisotropy (14) leads to $a_1 = d$ and $a_2^2 = 8K/\delta^2 J$ which correspond to the minimal model of Thio et al. [4]. In principle, the KSEA anisotropy (13) could lead to $a_1 \neq d$. However an estimate of the DM parameters D and D' within a tight-binding model [11] yields the near equality $|D| \approx |D'|$ which simplifies the diagonal elements of equation (13) to an Ising-like form, and thus $a_1 \approx d$, whereas the off-diagonal element K_{ab} does not appear in the effective theory. Another mechanism for $a_1 \neq d$ is provided by the diagonal nnn exchange anisotropies (see the Appendix) but we do not have a way to theoretically estimate those parameters. In short, departures from the strict equality $a_1 = d$ should be expected but the near equality $a_1 \approx d$ is likely a good assumption. In any case, our theoretical calculations will be carried out in terms of the three parameters (a_1, a_2, d) and further discussion of this issue is postponed to Section 4.3.

Next we discuss the field-dependent terms in equations (27) and (28). First we note the well-known fact that the last term in the free Lagrangian (27) breaks Lorentz invariance [17]. Incidentally, a mild breakdown of Lorentz invariance is also induced by the off-diagonal nnn exchange anisotropy discussed in the Appendix. The potential (28) contains two distinct contributions from the external field. The term $(\mathbf{n} \cdot \mathbf{h})^2$ is an easy-plane anisotropy due to the tendency of the two spins in a given dimer to antialign in a direction nearly perpendicular to the applied field. More subtle is the term $(\mathbf{h} \times \mathbf{d}) \cdot \mathbf{n}$ which couples the external field to the antisymmetric DM anisotropy. The existence of such a term was anticipated by Andreev and Marchenko [29] in their phenomenological treatment of conventional weak ferromagnets based on symmetry. Although this term is often dismissed in the literature [17], it was shown to be important for a

proper understanding of domain-wall dynamics [27]. In fact, the present work will provide ample evidence for the crucial importance of such a term in every aspect of weak ferromagnetism.

Whereas the complete physical picture cannot be established until we incorporate the interlayer coupling, in Section 4, the remainder of this section is devoted to the derivation of some basic consequences of the single-layer dynamics. Applications carried out in this paper pertain to homogeneous spin dynamics. One may then neglect spatial gradients to write

$$
\mathbf{m} = \frac{\delta}{4}[\mathbf{n} \times (\dot{\mathbf{n}} + \mathbf{d} - \mathbf{n} \times \mathbf{h})],
$$
$$
L_0 = \frac{1}{2}\dot{\mathbf{n}}^2 + \mathbf{h} \cdot (\mathbf{n} \times \dot{\mathbf{n}}),
$$
$$
V = (\mathbf{h} \times \mathbf{d}) \cdot \mathbf{n} + \frac{1}{2}(\mathbf{n} \cdot \mathbf{h})^2 + \frac{1}{2}(a_1^2 n_a^2 + a_2^2 n_c^2), \quad (30)
$$

which describe the low-frequency dynamics associated with the unit-cell Hamiltonian (16).

For our current demonstration we assume that the field points along the c axis ($h_a = 0 = h_b, h_c = h$) and thus the potential reduces to

$$
V = hdn_b + \frac{1}{2}[a_1^2 n_a^2 + (a_2^2 + h^2)n_c^2], \quad (31)
$$

whose local minima are given by $\mathbf{n} = (0, \mp 1, 0)$ and the corresponding magnetization is computed from the first equation in (30) applied for static $\mathbf{n}$; i.e , $\dot{\mathbf{n}} = 0$. Hence the two ground-state configurations are described by

$$
\mathbf{n} = \mp\mathbf{e}_b, \qquad \mathbf{m} = \frac{\delta}{4}(h \pm d)\mathbf{e}_c \quad (32)
$$

and are degenerate at zero field. For $h > 0$ the upper sign yields the absolute ground state, whereas the lower sign corresponds to a metastable local minimum with higher energy. Equation (32) makes it explicit that a weak ferromagnetic moment develops along the c axis even in the absence of an applied field.

The computation of the spectrum of normal frequencies is now straightforward. In terms of the standard angular variables

$$
n_a + in_b = \sin\Theta\, e^{i\Phi}, \qquad n_c = \cos\Theta, \quad (33)
$$

the free Lagrangian is written as

$$
L_0 = \frac{1}{2}(\dot{\Theta}^2 + \sin^2\Theta\,\dot{\Phi}^2) + h\sin^2\Theta\,\dot{\Phi}, \quad (34)
$$

and a corresponding angular parametrization of the potential is obtained simply by inserting equation (33) in (31).

The ground-state configurations are then given by $\Theta = \frac{\pi}{2}$, $\Phi = \mp\frac{\pi}{2}$, while small fluctuations are accounted for by making the replacements $\Theta = \frac{\pi}{2} - \theta$, $\Phi = \mp(\frac{\pi}{2} - \phi)$

and keeping terms that are at most quadratic in θ and ϕ. Also omitting a trivial additive constant and total derivatives one finds that

$$
L = L_0 - V \approx \frac{1}{2}(\dot{\phi}^2 + \dot{\theta}^2) - \frac{1}{2}(\omega_{1\pm}^2\phi^2 + \omega_{2\pm}^2\theta^2), \quad (35)
$$

where

$$
\omega_{1\pm}^2 = a_1^2 \pm hd, \qquad \omega_{2\pm}^2 = a_2^2 \pm hd + h^2 \quad (36)
$$

are the (squared) characteristic magnon frequencies for in-plane and out-of-plane fluctuations, respectively.

The actual experimental values of the calculated "magnon gaps" will be discussed in Section 4. But first we must fill a gap in our theoretical arguments concerning the choice of the scale parameter δ in equations (19)-(21). Although δ plays an important role in ascertaining the relative significance of the various terms that arise during the low-frequency reduction of the Landau-Lifshitz equations, consistency requires that all physical predictions be independent of δ. The magnon gaps (36) provide a good illustration of this point by recalling that the unit of frequency is $2s\delta J$. When the right-hand sides of equations (36) are multiplied by $(2s\delta J)^2$ the resulting expressions are indeed independent of δ and contain only the original microscopic parameters in suitable combinations. But one may exploit δ to choose more convenient rationalized units as discussed in Section 4.3.

This section is completed by quoting an explicit result for the corresponding dynamic susceptibilities. The method of calculation proceeds roughly as follows. Suppose that the system is found in its ground state in the presence of a constant field h along the c axis. A weak AC field of arbitrary direction and frequency ω is then turned on and the system eventually relaxes into a steady state oscillating with the same frequency thanks to the dissipative term present in equation (24). Once the steady state for the staggered moment $\mathbf{n}$ is determined from a perturbative solution of the nonlinear σ model, in the weak-AC-field limit, the magnetization $\mathbf{m}$ is calculated from the first equation in (30) to yield the sought after susceptibilities:

$$
\chi_{aa} = \frac{\delta}{4}\left[1 + \frac{\omega^2}{\omega_2^2 - \omega^2 - i\lambda\omega}\right],
$$

$$
\chi_{bb} = \frac{\delta}{4}\frac{(d+h)^2}{\omega_2^2 - \omega^2 - i\lambda\omega},
$$

$$
\chi_{cc} = \frac{\delta}{4}\left[1 + \frac{\omega^2}{\omega_1^2 - \omega^2 - i\lambda\omega}\right],
$$

$$
\chi_{ab} = -\chi_{ba} = \frac{i\delta}{4}\frac{(d+h)\omega}{\omega_2^2 - \omega^2 - i\lambda\omega},
$$

$$
\chi_{ac} = \chi_{ca} = \chi_{bc} = \chi_{cb} = 0, \quad (37)
$$

where ω_1 and ω_2 are the magnon gaps (36) restricted to the upper (+) sign; i.e., the gaps above the absolute

ground state when $h > 0$. The susceptibilities for the metastable ground state can be obtained by the universal replacement $h \to -h$. Since the two types of ground state mix in the presence of the interlayer coupling, the results of equations (36) and (37) should be interpreted with caution.

IV. INTERLAYER COUPLING

Although interlayer interactions are expected to be weak, they are important for a proper understanding of spin dynamics in La_2CuO_4. We have thus extended the symmetry analysis of Section 2 to include nn interlayer couplings on bonds that are parallel to either the ac or the bc plane. For each Cu atom there exist eight out-of-plane neighbors, four in the plane above and another four in the plane below. Symmetry requires that the isotropic exchange interaction is described by an exchange constant J_1 for bonds that are parallel to the ac plane, and a second exchange constant J_2 for bonds parallel to the bc plane. These two constants would be equal in the tetragonal ($I4/mmm$) phase but are different in the LTO phase due to the orthorhombic distortion.

The exchange constants are expected to individually satisfy the strong inequalities

$$J_1, J_2 \ll J, \tag{38}$$

in view of the fact that the length of out-of-plane nn bonds is significantly larger than the length of in-plane nn bonds. It is thus reasonable to assume that out-of-plane anisotropies (symmetric or antisymmetric) can be safely ignored because they are expected to be even weaker. In fact, we have worked out the form of all such anisotropies compatible with symmetry to convince ourselves that they do not bring in potentially new elements.

Therefore the three-dimensional (3D) unit-cell Hamiltonian can be written as

$$W_C^{3D} = W_C(\mathbf{A}, \mathbf{B}) + W_C(\boldsymbol{\Gamma}, \boldsymbol{\Delta}) + W_{int}(\mathbf{A}, \mathbf{B}, \boldsymbol{\Gamma}, \boldsymbol{\Delta}), \tag{39}$$

where the first term is the 2D unit-cell Hamiltonian (16), the second term is obtained by the simple substitution $(\mathbf{A}, \mathbf{B}) \to (\boldsymbol{\Gamma}, \boldsymbol{\Delta})$, and W_{int} contains the isotropic interlayer interactions. Simple inspection of Figure 1 leads to

$$W_{int} = 4J_1(\mathbf{A} \cdot \boldsymbol{\Gamma} + \mathbf{B} \cdot \boldsymbol{\Delta}) + 4J_2(\mathbf{A} \cdot \boldsymbol{\Delta} + \mathbf{B} \cdot \boldsymbol{\Gamma}). \tag{40}$$

This form is somewhat more involved than the one invoked by Thio et al. [5] but will eventually lead to the same physical picture.

We must now reformulate the strategy of Section 3 by introducing two pairs of variables

$$\mathbf{m}_1 = \frac{1}{2s}(\mathbf{A} + \mathbf{B}), \qquad \mathbf{n}_1 = \frac{1}{2s}(\mathbf{A} - \mathbf{B}),$$
$$\mathbf{m}_2 = \frac{1}{2s}(\boldsymbol{\Gamma} + \boldsymbol{\Delta}), \qquad \mathbf{n}_2 = \frac{1}{2s}(\boldsymbol{\Gamma} - \boldsymbol{\Delta}), \tag{41}$$

which would satisfy two identical copies of the 2D nonlinear σ model derived in Section 3 if the interlayer interaction (40) were neglected. The latter induces a coupling between the two copies which is especially simple if we invoke the strong inequalities (38). Then the magnetizations $\mathbf{m}_1$ and $\mathbf{m}_2$ are not directly affected by the interlayer coupling; i.e.,

$$\mathbf{m}_1 = \frac{\delta}{4}[\,\mathbf{n}_1 \times (\dot{\mathbf{n}}_1 + \mathbf{d} - \mathbf{n}_1 \times \mathbf{h})\,],$$
$$\mathbf{m}_2 = \frac{\delta}{4}[\,\mathbf{n}_2 \times (\dot{\mathbf{n}}_2 + \mathbf{d} - \mathbf{n}_2 \times \mathbf{h})\,], \tag{42}$$

but the staggered moments $\mathbf{n}_1$ and $\mathbf{n}_2$ satisfy a coupled dynamics described by the total Lagrangian

$$L = L_0 - V,$$
$$L_0 = L_{01} + L_{02}, \qquad V = V_1 + V_2 + V_{12}, \tag{43}$$

where L_{01} and L_{02} are two identical copies of the free Lagrangian of equation (30) applied for $\mathbf{n} = \mathbf{n}_1$ and $\mathbf{n} = \mathbf{n}_2$, respectively , V_1 and V_2 are similar copies of the 2D potential, and

$$V_{12} = \rho^2(\mathbf{n}_1 \cdot \mathbf{n}_2), \qquad \rho^2 \equiv \frac{8(J_1 - J_2)}{\delta^2 J}, \tag{44}$$

is an effective interlayer potential.

The further inequality $J_1 > J_2$ implied by the notation of equation (44) is simply an assumption consistent with phenomenology. To illustrate this assumption we consider the ground-state configuration(s) at zero external field. In this special case the absolute minimum of the total potential V of equation (43) is achieved when each term V_1, V_2 or V_{12} assumes its least possible value. Specifically, $\mathbf{n}_1 = -\mathbf{n}_2$ and

$$\mathbf{n}_1 = \mp \mathbf{e}_b, \qquad \mathbf{m}_1 = \pm \frac{\delta}{4} d \mathbf{e}_c,$$
$$\mathbf{n}_2 = \pm \mathbf{e}_b, \qquad \mathbf{m}_2 = \mp \frac{\delta}{4} d \mathbf{e}_c, \tag{45}$$

The spin configuration that corresponds to the upper sign is depicted in Figure 3, whereas the second ground state is obtained by reversing the sign of all spins and carries the same energy. In either case, the average total magnetization $\mathbf{m} = \frac{1}{2}(\mathbf{m}_1 + \mathbf{m}_2)$ vanishes and thus explains the term "covert weak ferromagnet" often employed to describe La_2CuO_4. More involved spin configurations arise in the presence of external fields and are described in Section 4.1 and 4.2.
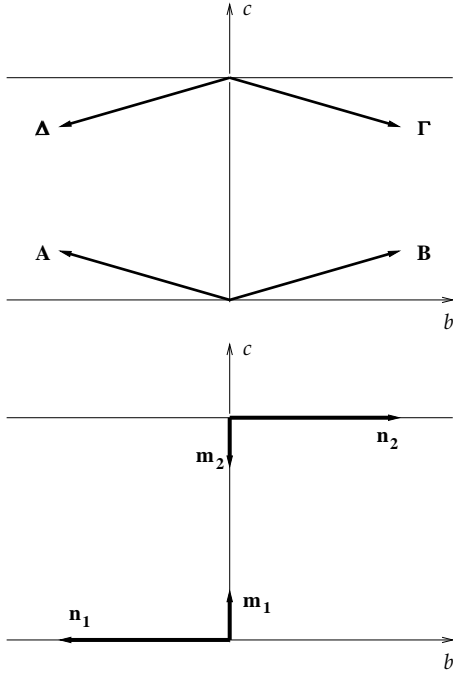
FIG. 3. Schematic representation of the ground-state configuration given by equation (45) with the upper sign. A second (degenerate) ground state is obtained by reversing the signs of all spins. The canting angle and the corresponding magnitude of $\mathbf{m}_1$ and $\mathbf{m}_2$ are greatly exaggerated for purposes of illustration.

This general description of the effective 3D dynamics is completed with three remarks :

(a) One would think that a more efficient formulation could be obtained in terms of the Dzyaloshinskii combination of fields [2]

$$\mathbf{m} = \frac{1}{2}(\mathbf{m}_1 + \mathbf{m}_2), \qquad \mathbf{n} = \frac{1}{2}(\mathbf{n}_1 + \mathbf{n}_2),$$
$$\mathbf{p} = \frac{1}{2}(\mathbf{m}_1 - \mathbf{m}_2), \qquad \mathbf{q} = \frac{1}{2}(\mathbf{n}_1 - \mathbf{n}_2), \qquad (46)$$

which arise naturally in a proper four-sublattice description of orthoferrites [26]. The latter are conventional weak ferromagnets with strong interlayer couplings which lead to $|\mathbf{m}|, |\mathbf{p}|, |\mathbf{q}| \ll |\mathbf{n}|$. One can then show that the effective low-frequency dynamics may be formulated with a single order parameter, the total staggered moment $\mathbf{n}$, and the remaining auxiliary fields $\mathbf{m}, \mathbf{p}$ and $\mathbf{q}$ are expressed in terms of $\mathbf{n}$ through algebraic relations similar to equation (42). However, such a formulation becomes singular when the interlayer exchange constants are much weaker than the intralayer one, as is assumed in equation (38). As a result, the current formulation in terms of two coupled order parameters $\mathbf{n}_1$ and $\mathbf{n}_2$ is more suitable.

(b) The assumed strong inequalities (38) also imply that gradient terms of any kind produce negligible corrections to the effective interlayer coupling. Therefore the homogeneous 3D dynamics described by equations (42)-(44) may be generalized to a complete continuum field theory simply by extending the free Lagrangians L_{01} and L_{02} to include 2D spatial gradients according to equation (27) applied for $\mathbf{n} = \mathbf{n}_1$ and $\mathbf{n} = \mathbf{n}_2$, respectively. The resulting field theory is essentially 2D and the only trace of 3D dynamics is the bilayer coupling (44).

(c) The interlayer potential (44) vanishes in the tetragonal phase ($J_1 = J_2$). Hence finer anisotropic couplings as well as quantum fluctuations are necessary to explain spin ordering [30] in, say, $Sr_2CuO_2Cl_2$ which remains tetragonal down to temperatures as low as 10 K [31]. A field theoretical description of these finer couplings is not available at present and thus the isotropic 2D nonlinear σ model is the main tool for investigation of tetragonal compounds [32].

A. Weak-ferromagnetic transition

We return to the problem posed in the concluding paragraphs of Section 3 and now address it within its proper 3D context. When a field of strength h is applied along the c axis the total bilayer potential is given by

$$V = \rho^2(\mathbf{n}_1 \cdot \mathbf{n}_2) + hd(n_{1b} + n_{2b})$$
$$+ \frac{1}{2}[a_1^2(n_{1a}^2 + n_{2a}^2) + (a_2^2 + h^2)(n_{1c}^2 + n_{2c}^2)], \quad (47)$$

where $\mathbf{n}_1 = (n_{1a}, n_{1b}, n_{1c})$ and $\mathbf{n}_2 = (n_{2a}, n_{2b}, n_{2c})$ are the two order parameters expressed in Cartesian components. Simple inspection of the potential, taking into account that $a_1 < a_2$, suggests that its minima are such that $n_{1c} = 0 = n_{2c}$. One may then parametrize the remaining components as $(n_{1a}, n_{1b}) = (\cos \Phi_1, \sin \Phi_1)$ and $(n_{2a}, n_{2b}) = (\cos \Phi_2, \sin \Phi_2)$ to obtain

$$V = \rho^2 \cos(\Phi_1 - \Phi_2) + hd(\sin \Phi_1 + \sin \Phi_2)$$
$$+ \frac{1}{2}a_1^2(\cos^2 \Phi_1 + \cos^2 \Phi_2). \quad (48)$$

This reduced potential reveals an interesting formal analogy to the case of an easy-axis antiferromagnet with exchange constant ρ^2, anisotropy a_1^2, and an effective field of strength hd applied along the easy b axis; even though the actual field points along the c axis.

Therefore the search for the minima of (48) follows the familiar pattern of the conventional spin-flop transition in an easy-axis classical antiferromagnet, with due attention to the fact that the relevant order parameters are now the staggered moments and not the actual spins. The results of this straightforward minimization problem can be simply stated by introducing the temporary notational abbreviations

$$X = \frac{hd}{\rho^2}, \qquad Y = \frac{a_1^2}{\rho^2}, \qquad (49)$$

and are summarized in the $T = 0$ phase diagram of Figure 4 supplemented by the typical configurations within each phase illustrated in Figure 5.
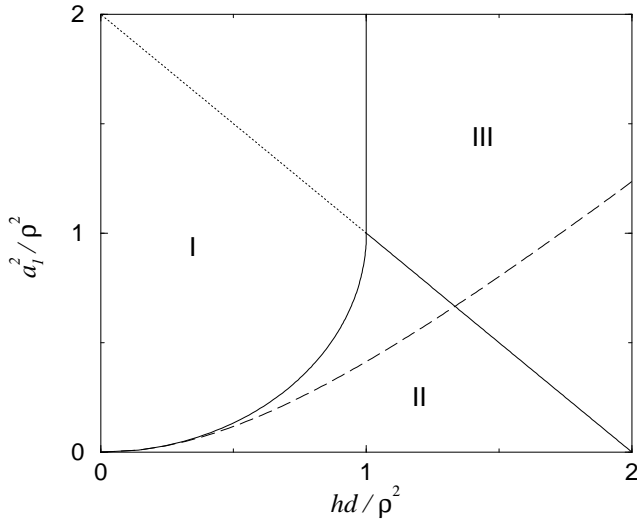
8

FIG. 4. The $T = 0$ phase diagram for a field h parallel to the c axis. The true critical boundaries are depicted by solid lines, the limit of local stability of Phase I is shown by a dashed line, and the same limit of Phase III by a dotted line. The WF transition in La_2CuO_4 is described by the first-order I : III transition.
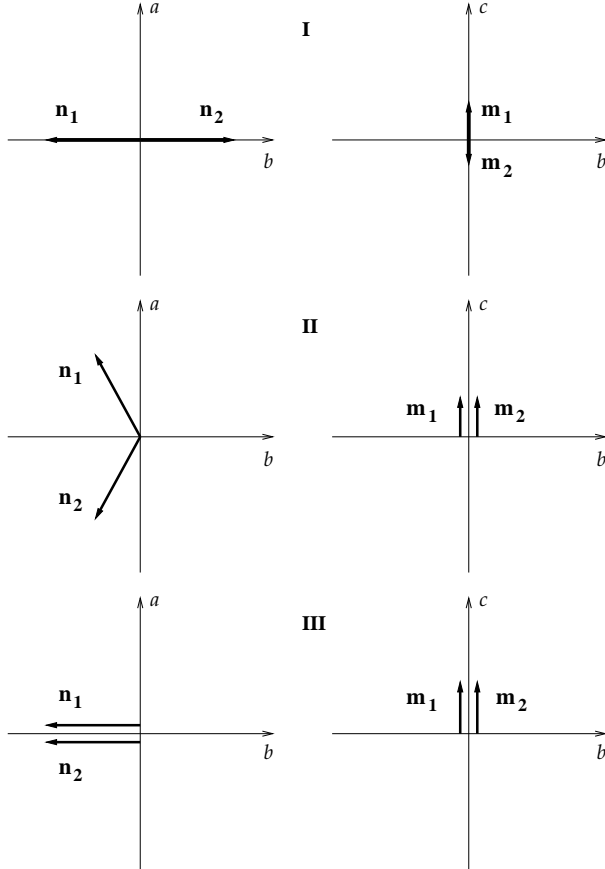

FIG. 5. Representative ground-state configurations in Phases I, II, and III of the $T = 0$ phase diagram of Figure 4. In all three cases the net magnetization $\mathbf{m} = \frac{1}{2}(\mathbf{m}_1 + \mathbf{m}_2)$ points along the field direction (c axis).

At zero field ($X = 0$) the ground state is given by equation (45) and exhibits twofold degeneracy. It is sufficient to consider the configuration defined by the upper sign in (45) and follow its evolution at nonvanishing field h:

$$\mathbf{n}_1 = -\mathbf{e}_b, \qquad \mathbf{m}_1 = \frac{\delta}{4}(h + d)\mathbf{e}_c,$$
$$\mathbf{n}_2 = +\mathbf{e}_b, \qquad \mathbf{m}_2 = \frac{\delta}{4}(h - d)\mathbf{e}_c,$$
$$\mathbf{m} = \frac{1}{2}(\mathbf{m}_1 + \mathbf{m}_2) = \frac{\delta}{4}h\mathbf{e}_c, \qquad (50)$$

which is depicted in entry I of Figure 5 and exhibits a net moment $\mathbf{m}$ along the c axis whose magnitude increases linearly with the applied field.

Configuration I remains locally stable until the field crosses the boundary

$$Y = \sqrt{1 + X^2} - 1 \qquad (51)$$

shown by a dashed line in the phase diagram of Figure 4. However this state becomes metastable at an earlier stage and the true critical boundary of Phase I consists of two branches:

$$Y = 1 - \sqrt{1 - X^2}, \qquad X < 1, \qquad (52)$$

and

$$X = 1, \qquad Y > 1, \qquad (53)$$

which are drawn by solid lines in Figure 4 and join a third critical line

$$X + Y = 2, \qquad Y < 1, \qquad (54)$$

at the "tricritical" point $X = 1 = Y$.

For anisotropies below the tricritical point ($Y < 1$) the system would undergo a first-order transition at the critical line (52) to enter Phase II characterized by a flopped configuration of the staggered moments $\mathbf{n}_1$ and $\mathbf{n}_2$ but magnetizations $\mathbf{m}_1$ and $\mathbf{m}_2$ that are both aligned along the c axis. With further increase of the applied field beyond the critical boundary (54) a second-order transition occurs and the system enters Phase III in which both staggered moments are parallel to the (negative) b axis.

As we will see in Section 4.3, the parameters of La_2CuO_4 favor the value $Y = a_1^2/\rho^2 \approx 2$ and hence the relevant weak-ferromagnetic (WF) transition is the direct I : III transition that occurs at the critical line (53), or at a critical field $h = h_0$ given by

$$h_0 = \rho^2/d. \qquad (55)$$

The WF transition is clearly first order because the boundary of local stability of Phase I shown by a dashed line in Figure 4 extends well to the right of the true critical boundary (53). Similarly the boundary of local stability of Phase III shown by a dotted line extends well to the left of the true critical boundary.

9

One may express equation (55) in terms of the original variables to write

$$mH_0 = s^2 J_\perp, \qquad J_\perp \equiv 4(J_1 - J_2), \qquad (56)$$

where H_0 is the critical field, m is the weak moment per Cu atom at zero field, $s = 1/2$ is the spin of a Cu^{2+} ion, and $J_\perp$ is an effective interlayer exchange constant. With this identification of $J_\perp$ equation (56) coincides with the original estimate of Thio et al. [4]. In oxygen-doped La_2CuO_{4+y} samples of reduced Néel temperature ($T_N \sim 240K$) the measured critical field is $H_0 = 5T$, $m = 2.1 \times 10^{-3} \mu_B$, and thus $J_\perp$ is estimated to be $2.5 \mu eV$.

The description of the general features of the WF transition is completed by quoting the explicit ground-state configuration in Phase III:

$$\mathbf{n}_1 = -\mathbf{e}_b = \mathbf{n}_2,$$
$$\mathbf{m} = \mathbf{m}_1 = \mathbf{m}_2 = \frac{\delta}{4}(d+h)\mathbf{e}_c, \qquad (57)$$

where the net moment $\mathbf{m}$ again increases linearly with h. The results for the net magnetization in Phases I and III, given by equations (50) and (57), are shown by a dashed line in Figure 6 which exhibits a sudden jump at the critical field $H_0 = 5T$ due to the first-order nature of the WF transition. One should stress that this calculation is strictly valid at $T = 0$; the magnetization jump is increasingly smoothed out with rising temperature [4,5].
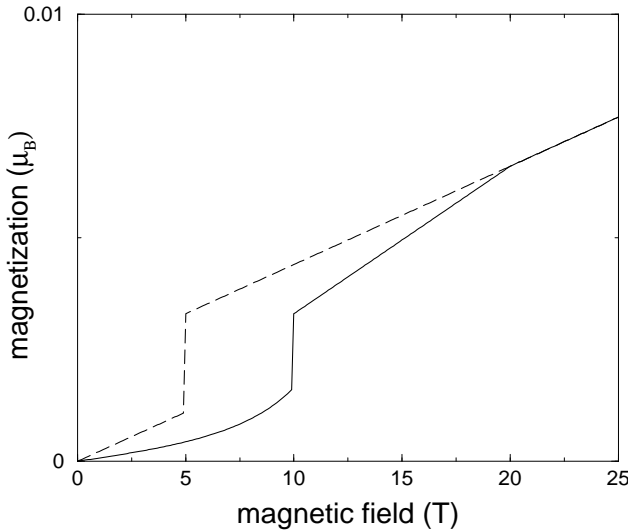

FIG. 6. Net magnetization induced by an applied field. The dashed line corresponds to a field along the c axis and demonstrates the WF transition at the critical field $H_0 = 5T$. The solid line corresponds to a field along the b axis and displays discontinuities at the critical fields $H_1 = 10T$ and $H_2 = 20T$ characteristic of the SF transition. In either case the net magnetization points along the direction of the applied field.

It is now interesting to recalculate the magnon gaps in the presence of the interlayer coupling and follow them through the WF transition. If we parametrize $\mathbf{n}_1$ and $\mathbf{n}_2$ by two replicas of the angular variables (33) the ground-state configuration in Phase I is given by $(\Theta_1 = \frac{\pi}{2}, \Phi_1 = -\frac{\pi}{2})$ and $(\Theta_2 = \frac{\pi}{2}, \Phi_2 = \frac{\pi}{2})$. Small fluctuations are then studied by introducing the variables $(\Theta_1 = \frac{\pi}{2} - \theta_1, \Phi_1 = -\frac{\pi}{2} + \phi_1)$ and $(\Theta_2 = \frac{\pi}{2} - \theta_2, \Phi_2 = \frac{\pi}{2} - \phi_2)$ in the complete Lagrangian (43) and keeping terms that are at most quadratic :

$$L \approx \frac{1}{2}(\dot\phi_1^2 + \dot\phi_2^2 + \dot\theta_1^2 + \dot\theta_2^2) - \rho^2(\phi_1\phi_2 + \theta_1\theta_2)$$
$$- \frac{1}{2}(c_1^+\phi_1^2 + c_1^-\phi_2^2 + c_2^+\theta_1^2 + c_2^-\theta_2^2),$$

$$c_1^\pm \equiv a_1^2 \pm hd + \rho^2, c_2^\pm \equiv a_2^2 \pm hd + h^2 + \rho^2. \quad (58)$$

Standard diagonalization of this quadratic form yields the four magnon gaps

$$\Omega_{1\pm}^2 = a_1^2 + \rho^2 \pm \sqrt{h^2 d^2 + \rho^4},$$

$$\Omega_{2\pm}^2 = a_2^2 + \rho^2 \pm \sqrt{h^2 d^2 + \rho^4} + h^2, \qquad (59)$$

which reduce to the gaps of equation (36) at zero interlayer coupling ($\rho^2 = 0$). The zero-field limit of equation (59) is also interesting and leads to

$$\Omega_{1-} = a_1, \qquad\qquad \Omega_{2-} = a_2,$$

$$\Omega_{1+} = \sqrt{a_1^2 + 2\rho^2}, \qquad \Omega_{2+} = \sqrt{a_2^2 + 2\rho^2}. \qquad (60)$$

The "acoustical" gaps 1^- and 2^- do not depend on the interlayer coupling and correspond to the usual antiferromagnetic (AF) modes for in-plane and out-of-plane fluctuations, respectively. The "optical" gaps 1^+ and 2^+ are sensitive to the interlayer coupling and may be said to correspond to exchange (E) modes, in analogy with a similar distinction made within a proper four-sublattice formulation of orthoferrites [26]. In the latter case, AF and E modes are widely separated thanks to a strong interlayer exchange interaction that is comparable to the intralayer one. In contrast, a close proximity of these two types of modes should be expected in La_2CuO_4 because $2\rho^2 \approx a_1^2$.

The decoupling of AF and E modes suggested by equation (60) no longer holds in the presence of an applied field, as is apparent in equation (59). In this respect, it is also useful to follow the gaps beyond the WF transition. In Phase III the ground-state configuration is given by $\Theta_1 = \frac{\pi}{2} = \Theta_2$, $\Phi_1 = -\frac{\pi}{2} = \Phi_2$ and small fluctuations lead to a quadratic Lagrangian similar to (58). The corresponding magnon gaps are found to be

$$\Omega_{1-}^2 = a_1^2 + hd - 2\rho^2,$$

10

$$\Omega_{2-}^2 = a_2^2 + hd + h^2 - 2\rho^2,$$

$$\Omega_{1+}^2 = a_1^2 + hd,$$

$$\Omega_{2+}^2 = a_2^2 + hd + h^2, \qquad (61)$$

where the role of acoustical and optical modes is clearly interchanged. To be sure, equation (59) is valid for $h < h_0$ and equation (61) for for $h > h_0$. The spectrum exhibits a discontinuity at $h = h_0$ thanks again to the first-order nature of the WF transition.

The calculation of dynamic susceptibilities can be effected by the method briefly outlined in the concluding paragraph of Section 3 within the simpler 2D context. We do not present here explicit results in order to avoid further proliferation of algebraic formulas. But such results can be provided should the need arise.

B. Spin-flop transition

The case of a field applied along some direction in the basal plane is equally interesting. In particular, when the field is precisely aligned with the b axis, an unusual spin-flop (SF) transition is reflected in magnetoresistance measurements [5]. An important element in the corresponding theoretical analysis is that the observed in-plane magnon gap is smaller than the out-of-plane gap ($a_1 < a_2$).

The total bilayer potential in a field $\mathbf{h} = (0, h, 0)$ is given by

$$V = \rho^2(\mathbf{n}_1 \cdot \mathbf{n}_2) - hd(n_{1c} + n_{2c}) + \frac{1}{2}h^2(n_{1b}^2 + n_{2b}^2)$$
$$+ \frac{1}{2}[a_1^2(n_{1a}^2 + n_{2a}^2) + a_2^2(n_{1c}^2 + n_{2c}^2)] \qquad (62)$$

Inspite first appearances minimization of the above potential is straightforward. The two unit vectors $\mathbf{n}_1$ and $\mathbf{n}_2$ are parametrized in terms of two sets of angular variables (Θ_1, Φ_1) and (Θ_2, Φ_2). One can then show that the minima of (62) are such that

$$\Theta_1 = \Theta_2 = \Theta \qquad (63)$$

for any value of the applied field. However the azimuthal angles Φ_1 and Φ_2 display different behavior in three distinct field regions separated by two critical fields:

$$h_1 = a_1, \qquad h_2 = \frac{1}{d}(a_2^2 + 2\rho^2 - a_1^2). \qquad (64)$$

For $h < h_1$ the ground-state configuration is illustrated in the first entry of Figure 7. The staggered moments are both contained in the bc plane and cant toward the c axis with which they form an angle Θ given by
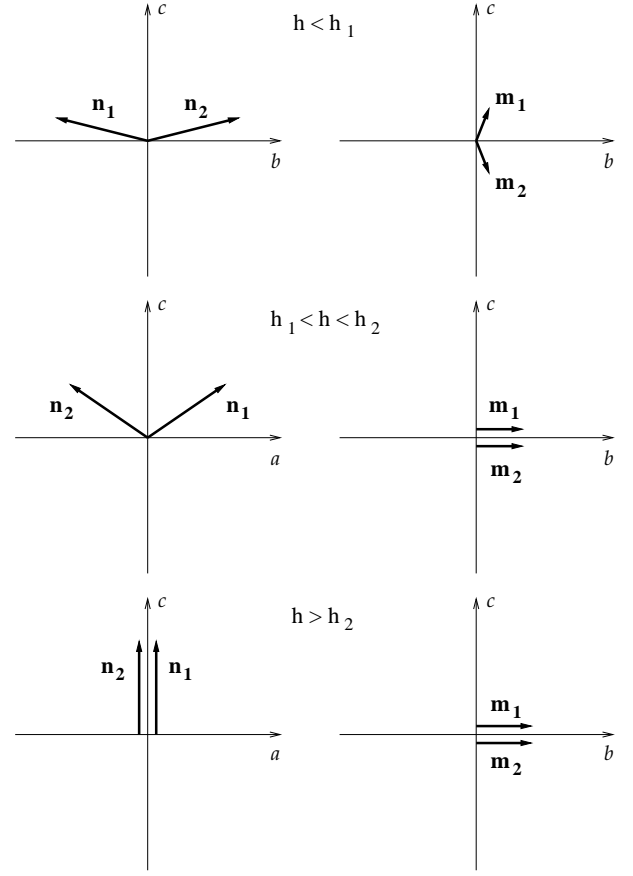

FIG. 7. Representative ground-state configurations in the three distinct field regions that characterize the SF transition. In all three cases the net magnetization $\mathbf{m} = \frac{1}{2}(\mathbf{m}_1 + \mathbf{m}_2)$ points in the direction of the applied field (b axis).

$$\cos\Theta = \frac{hd}{a_2^2 + 2\rho^2 - h^2}. \qquad (65)$$

Accordingly the net magnetization points along the direction of the applied field, namely

$$\mathbf{m} = \frac{1}{2}(\mathbf{m}_1 + \mathbf{m}_2) = \frac{\delta}{4}(d + h\cos\Theta)\cos\Theta\,\mathbf{e}_b. \qquad (66)$$

For $h_1 < h < h_2$ the staggered moments flop into the ac plane and form an angle with the c axis given by

$$\cos\Theta = \frac{hd}{a_2^2 + 2\rho^2 - a_1^2}, \qquad (67)$$

while the corresponding net magnetization is

$$\mathbf{m} = \mathbf{m}_1 = \mathbf{m}_2 = \frac{\delta}{4}(h + d\cos\Theta)\mathbf{e}_b. \qquad (68)$$

Finally, for $h > h_2$, both staggered moments are aligned with the c axis but the net magnetization

$$\mathbf{m} = \mathbf{m}_1 = \mathbf{m}_2 = \frac{\delta}{4}(d + h)\mathbf{e}_b \qquad (69)$$

continues to point along the field direction. This picture should be completed with the remark that the calculated

11

sharp SF transition at the critical fields h_1 and h_2 is smoothed out when the direction of the applied field departs from the b axis.

The preceding description of the SF transition confirms the theoretical analysis of Thio et al. which was in turn shown to be consistent with experiment [5]. In particular, the critical fields (64) agree with those of reference [5] if we adopt the minimal choice $a_1 = d$ and identify the effective interlayer exchange constant $J_\perp$ as in equation (56). The net magnetization calculated from equations (66), (68) and (69) is depicted by a solid line in Figure 6 and displays characteristic discontinuities at the observed critical fields $H_1 = 10T$ and $H_2 = 20T$. A minor difference in the overall scale of Figure 6 with the corresponding result of reference [5] is apparently due to a slightly different choice of parameters, as discussed in the following subsection.

C. Rationalized units and constants

Our purpose here is to demonstrate how to efficiently use the rationalized formulas derived throughout this paper, rather than to analyze in depth the available experimental data. Such an analysis is complicated by the fact that actual experiments have been performed on samples with varying oxygen doping. Pure La_2CuO_4 samples have been available [1,32] and exhibit magnetic order below the Néel temperature $T_N = 325K$. However the most complete set of magnetic measurements was obtained on oxygen-doped La_2CuO_{4+y} with reduced Néel temperature [4,5]. Hence our demonstration will be based on the latter measurements but could be extended to pure samples in a straightforward manner.

We begin with a parameter-free theoretical prediction based on the fact that the first critical field in equation (64) and the zero-field 1^- gap in equation (60) are both equal to a_1. In physical units this equality reads $g_m\mu_B H_1 = \Omega_{1-}$ where $g_m = 2.2$ is the gyromagnetic ratio and μ_B the Bohr magneton. Hence, if we use the measured critical field $H_1 = 10.5 \pm 1T$, the predicted in-plane gap $\Omega_{1-} = 1.33 \pm 0.12meV$ is consistent with the measured $1.1 \pm 0.3meV$. For simplicity we adopt in the following the rounded critical field value $H_1 = 10T$ which leads to $\Omega_{1-} = 1.27meV$.

Now the theoretical zero-field weak moment per Cu atom is $m = \delta d/4$ or, in physical units, $m = sg_m\mu_B\delta d/4$ which should be compared to a measured value $2.2 \times 10^{-3}\mu_B$ to yield $\delta d = 8 \times 10^{-3}$. This is an estimate of the DM anisotropy recalling that $\delta d = 2D/J$. However a more convenient framework is obtained by exploiting the scale parameter δ to *define* rationalized units such that $d \equiv 1$, and thus $\delta = 8 \times 10^{-3}$, as anticipated by the discussion of Section 3. For the moment we restrict attention to the minimal model for which $a_1 = d \equiv 1$. Hence the theoretical critical field $h_1 = a_1 = 1$ sets the

rationalized field unit equal to the measured $H_1 = 10T$, and the theoretical in-plane gap $\Omega_{1-} = a_1 = 1$ sets the unit of frequency at $1.27meV$. Then the measured critical field for the WF transition $H_0 = 5T$ is translated into $h_0 = 1/2$ rationalized units and thus equation (55) reads $h_0 = \rho^2/d = \rho^2 = 1/2$ which provides a rationalized estimate of the interlayer coupling. Finally we consider the theoretical critical field h_2 of equation (64) which may now be applied with $a_1 = d = 1$ and $2\rho^2 = 1$ to yield $h_2 = a_2^2$ in rationalized units or $H_2 = 10a_2^2 T$ in physical units. Comparing this prediction to the measured critical field $H_2 = 20T$ we find that $a_2 = \sqrt{2}$.

To summarize, all theoretical formulas may be applied with rationalized parameters

$$\delta = 8 \times 10^{-3}; \quad a_1 = d \equiv 1, \quad a_2 = \sqrt{2}, \quad \rho^2 = \frac{1}{2}, \quad (70)$$

supplemented by the stipulation that the physical unit for frequency be $1.27meV$, for field $10T$, and for magnetization $sg_m\mu_B = 1.1\mu_B$.

The *predicted* values for the acoustical gaps $\Omega_{1-} = 1.27a_1 = 1.27meV$ and $\Omega_{2-} = 1.27a_2 = 1.8meV$ are marginally consistent with the observed $1.1 \pm 0.3meV$ and $2.5 \pm 0.5meV$. In fact, full consistency would be restored if we had included error bars in our analysis [5] instead of the conveniently rounded input values for the critical fields and the magnetization actually used in our demonstration. Furthermore the optical gaps of equation (60) are now predicted to be $\Omega_{1+} = 1.27\sqrt{a_1^2 + 2\rho^2} = 1.8meV$ and $\Omega_{2+} = 1.27\sqrt{a_2^2 + 2\rho^2} = 2.2meV$. We do not know of an experimental determination of the optical gaps. Thus we merely note the predicted close proximity of acoustical and optical gaps, as anticipated in Section 4.1.

Since the unit of frequency is equal to $2s\delta J = \delta J = 1.27meV$, the exchange constant is predicted to be $J = 1.27/\delta = 158meV$. Curiously, this classical value of the exchange constant is the same with the one obtained in Section 3 in relation to the spinwave velocity $850meV\mathring{A}$ observed on pure ($T_N = 325K$) samples. But the spinwave velocity on oxygen-doped samples is typically lower ($\sim 700meV\mathring{A}$) and thus the currently predicted classical J is somewhat uncomfortably high. One would think that such a discrepancy can be averted by resorting to a nonminimal model with $a_1 \neq d$. Interestingly, a more comfortable value of J can thus be obtained but only at the expense of further deterioration (lowering) of the prediction for the out-of-plane acoustical gap $\Omega_{2-} = 1.8meV$ discussed in the preceding paragraph; and vice versa. Putting it differently, current data do not indicate departure from the minimal model $a_1 = d$.

The overall consistency is satisfactory in view of the following limiting circumstances:

(a) The theoretical model is strictly valid for pure La_2CuO_4 and its application to oxygen-doped samples

should be viewed with caution. Unfortunately, a complete set of magnetic measurements is not available on pure samples probably because the observed magnon gaps are nearly doubled [1] and thus the critical fields required to induce the SF transition become prohibitively intense.

(b) The theoretical calculation is strictly valid at $T = 0$. Although the measured magnetization and critical fields [4,5] have been extrapolated to $T = 0$, other quantities such as the magnon gaps are typically determined at relatively high temperatures ($T \sim 100K$).

(c) The assumption of strictly localized spins is always in question, and the further use of a classical description is marginal for this low spin value ($s = 1/2$) and low effective lattice dimension (D = 2). Since different physical quantities are renormalized differently by quantum fluctuations, including calculated quantum-renormalization factors into the classical predictions can be confusing [32].

V. CONCLUSION

While the phenomenological picture derived by Thio et al. [4–6] is confirmed by the present analysis, some new elements have emerged that may deserve closer attention:

The structure of the magnon gaps is more involved than normally assumed because of the underlying four-sublattice magnetic ground state. The calculated acoustical and optical gaps are not widely separated and hybridization takes place in the presence of external fields. Therefore study of the field-dependence of the magnon gaps may lead to further tests of the derived picture.

The description of the isotropic 2D antiferromagnet in terms of a relativistic nonlinear σ model has already provided interesting results [15,16] but the presence of anisotropies and an interlayer coupling are clearly important for a more detailed understanding of the magnetic structure of La_2CuO_4. Suffice it to say that the existence of a finite Néel temperature ($T_N = 325K$) is precisely due to such perturbations. Hence it is conceivable that the field theoretical framework discussed here may help to address some of the remaining questions [32].

The covert nature of weak ferromagnetism in La_2CuO_4 makes it difficult to directly observe macroscopic magnetic domains. Nevertheless, even on structurally pure samples, cooling below T_N should produce numerous magnetic domains and antidomains separated by domain walls that are invisible because the average magnetization vanishes at zero external field. When a field is applied in a direction perpendicular to the CuO_2 planes domain walls evolve into magnetic stripes that exhibit enhanced magnetization over a region of finite width and could thus become visible. Static magnetic stripes are stable for field strengths smaller than the critical value H_0 required to induce the WF transition, thanks to the restoring force supplied by the antiferromagnetic interlayer coupling. When the field exceeds H_0 stripes are rendered unstable and begin to expand steadily in both directions, thus providing a detailed mechanism for the observed first-order WF transition.

The preceding qualitative picture may be put on a firm quantitative basis using the derived continuum field theory, as we hope to demonstrate in a future publication.

APPENDIX A: NNN IN-PLANE INTERACTIONS

Here we consider the modifications of the 2D Hamiltonian of Section 2 that result from spin interactions along the diagonals of the Cu plaquettes. Symmetry precludes the existence of antisymmetric DM anisotropies on such bonds and thus all nnn contributions to the Hamiltonian may be cast in the form

$$W_{nnn} = \frac{1}{2} \sum_{\ll kl \gg} \sum_{i,j} G_{kl}^{ij}(S_k^i S_l^j + S_k^j S_l^i) \qquad (A1)$$

where $\ll kl \gg$ denotes a nnn bond and the symmetric matrices $G_{kl} = (G_{kl}^{ij})$ are *not* assumed to be traceless. The possible value of G_{kl} are again restricted by symmetry as shown in Figure 8. Thus A spins interact with their A neighbors through the exchange matrices

$$G_1 = \begin{pmatrix} G_{1aa} & 0 & 0 \\ 0 & G_{1bb} & G_{1bc} \\ 0 & G_{1bc} & G_{1cc} \end{pmatrix},$$

$$G_2 = \begin{pmatrix} G_{2aa} & 0 & 0 \\ 0 & G_{2bb} & G_{2bc} \\ 0 & G_{2bc} & G_{2cc} \end{pmatrix}, \qquad (A2)$$

along the a and b direction, respectively, whereas B spins interact with exchange matrices

$$G_1' = \begin{pmatrix} G_{1aa} & 0 & 0 \\ 0 & G_{1bb} & -G_{1bc} \\ 0 & -G_{1bc} & G_{1cc} \end{pmatrix},$$

$$G_2' = \begin{pmatrix} G_{2aa} & 0 & 0 \\ 0 & G_{2bb} & -G_{2bc} \\ 0 & -G_{2bc} & G_{2cc} \end{pmatrix}, \qquad (A3)$$

which are related to G_1 and G_2. A corollary of these symmetry relations is that the isotropic components of nnn exchange couplings, given by the traces of the above matrices, are characterized by two exchange constants which are generally different along the a and b directions but the same for AA and BB bonds.
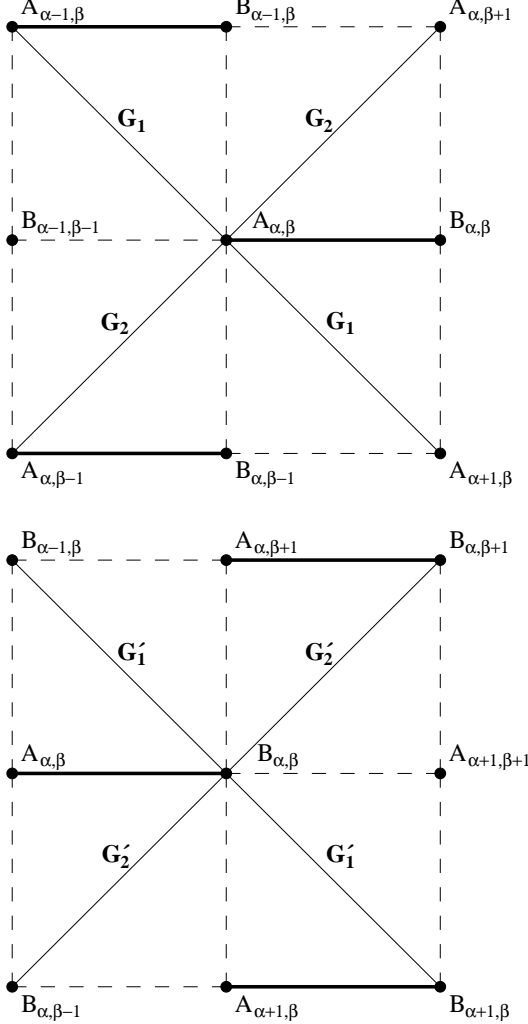

FIG. 8. Illustration of the distribution of the matrices G and G' given in the Appendix. These symmetric matrices describe nnn exchange interactions along the diagonals of the Cu plaquettes which are parallel to the a and b axes. The remaining conventions are those of Figure 2.

The corresponding modifications of the effective low-frequency dynamics may be briefly summarized as follows. The traces of the above matrices introduce an overall additive renormalization of the isotropic exchange constant J. Similarly the contributions from the diagonal anisotropies submerge with the anisotropy constants a_1 and a_2 already discussed in the main text. The only new parameter is then introduced by the off-diagonal anisotropy, namely

$$g = \frac{G_{1bc} + G_{2bc}}{\delta J}, \qquad \mathbf{G} \equiv g(n_c \mathbf{e}_b + n_b \mathbf{e}_c), \quad (A4)$$

where we have also defined a vector $\mathbf{G}$ that depends on the staggered moment but plays a role similar to the DM vector $\mathbf{d} = d\mathbf{e}_a$. Then equations (30) generalize to

$$\mathbf{m} = \frac{\delta}{4}[\mathbf{n} \times (\dot{\mathbf{n}} + \mathbf{d} + \mathbf{n} \times \mathbf{G} - \mathbf{n} \times \mathbf{h})],$$

$$L_0 = \frac{1}{2}\dot{\mathbf{n}}^2 + \frac{3}{2}g(n_b^2 - n_c^2)\dot{n}_a + \mathbf{h} \cdot (\mathbf{n} \times \dot{\mathbf{n}}),$$

$$V = (\mathbf{h} \times \mathbf{d}) \cdot \mathbf{n} + g[h_c n_b + h_b n_c - 2(\mathbf{n} \cdot \mathbf{h})n_b n_c] + \frac{1}{2}(\mathbf{n} \cdot \mathbf{h})^2 + \frac{1}{2}(a_1^2 n_a^2 + a_2^2 n_c^2) + 2g^2 n_b^2 n_c^2, \quad (A5)$$

which were actually used throughout our analysis. But the results presented in the main text were restricted to $g = 0$ mainly because the qualitative picture remains intact and current experimental data are not sufficiently accurate or detailed to discern a nonvanishing g.

[a]   Electronic address: papanico@physics.uoc.gr

[1] M. E. Kastner, R. J. Birgeneau, G. Shirane, Y.Endoh, Rev. Mod. Phys. **70**, 897 (1998).

[2] I. Dzyaloshinskii, Phys. Chem. Solids **4**, 241 (1958).

[3] T. Moriya, Phys. Rev. **120**, 91 (1960).

[4] T.Thio, T. R. Thurston, N. W. Preyer, P. J. Picone, M. A. Kastner, H. P. Jenssen, D. R. Gabbe, C. Y. Chen, R. J. Birgeneau, A. Aharony, Phys. Rev. B **38**, 905 (1988).

[5] T. Thio, C. Y. Chen, B. S. Freer, D. R. Gabbe, H. P. Jenssen, M. A. Kastner, P. J. Picone, N. W. Preyer, R. J. Birgeneau, Phys. Rev. B **41**, 231 (1990).

[6] T. Thio, A. Aharony, Phys. Rev. Lett. **73**, 894 (1994).

[7] D. Coffey, K. S. Bedell, S. A. Trugman, Phys. Rev. B **42**, 6509 (1990).

[8] D. Coffey, T. M. Rice, F. C. Zhang, Phys. Rev. B **44**, 10112 (1991)

[9] T. A. Kaplan, Z. Phys B **49**, 313 (1983).

[10] L. Shekhtman, O. Entin-Wohlman, A. Aharony, Phys. Rev. Lett. **69**, 836 (1992).

[11] L. Shekhtman, A. Aharony, O. Entin-Wohlman, Phys. Rev. B **47**, 174 (1993).

[12] A. Zheludev, S. Maslov, G. Shirane, I. Tsukada, T. Masuda, K. Uchinokura, I. Zaliznyak, R. Erwin, L. P. Regnault, Phys. Rev. B **59**, 11432 (1999).

[13] B. I. Halperin, P. C. Hohenberg, Phys. Rev. **188**, 898 (1969).

[14] D. Forster, *Hydrodynamic Fluctuations,Broken Symmetry, and Correlation Functions* (Benjamin, Reading, 1975).

[15] S. Chakravarty, B. I. Halperin, D. R. Nelson, Phys. Rev. B **39**, 2344 (1989).

[16] P. Hasenfratz, F. Niedermayer, Phys. Lett. B **268**, 231 (1991).

[17] V. G. Bar'yakhtar, M. V. Chetkin, B. A. Ivanov, S. N. Gadetskii, *Dynamics of Topological Magnetic Solitons - Experiment and Theory* (Springer Verlag, Berlin, 1994).

[18] C. Retorri, D. Rao, S. B. Oseroff, G. Amoretti, Z. Fisk, S-W. Cheong, D. Vier, S. Schultz, M. Tovar, R. D. Zysler, J. E. Schirber, Phys. Rev. B **47**, 8156 (1993).

[19] A. V. Bazhenov, C. B. Rezchikov, I. S. Smirnova, Physica C **273**, 9 (1996).

[20] D. Vaknin, S. K. Sinha, D.E. Moncton, D. C. Johnston, J. M. Newsam, C. R. Safiniya, H. E. King Jr., Phys. Rev. Lett **58**, 2802 (1987).

[21] J. Lorenzana, J. Eroles, S. Sorella, Phys. Rev. Lett. **83**, 5122 (1999).

[22] T. Yildirim, A. B. Harris, A. Aharony, O. Entin-Wohlman, Phys. Rev. B **52**, 10239 (1995).

[23] L. Landau, E.Lifshitz, Phys. Z. Sov. Union **8**, 153 (1935).

[24] T. L. Gilbert, Phys. Rev. **100**, 1243 (1955).

[25] G. F. Herrmann, J. Phys. Chem. Solids **24**, 597 (1963).

[26] G. F. Herrmann, Phys. Rev. **133**, A1334 (1964).

[27] N. Papanicolaou, Phys. Rev. B **55**, 12 290 (1997).

[28] S. Komineas, N. Papanicolaou, Nonlinearity **11**, 265 (1998).

[29] A. F. Andreev, V. I. Marchenko, Sov. Phys. Usp. **23**, 21 (1980).

[30] T. Yildirim, A. B. Harris, O. Entin-Wohlman, A. Aharony, Phys. Rev. Lett. **72**, 3710 (1994).

[31] M. Greven, R. J. Birgeneau, Y. Endoh, M. A. Kastner, M. Matsuda, G. Shirane, Z.Phys. B **96**, 465 (1995).

[32] R. J. Birgeneau, M. Greven, M. A. Kastner, Y. S. Lee, B. O. Wells, Y. Endoh, K. Yamada, G. Shirane, Phys. Rev. B **59**, 13 788 (1999).